

ICNTS - Benchmarking of Bootstrap Current Coefficients

Klaus ALLMAIER¹⁾, Craig D. BEIDLER²⁾, Maxim Yu. ISAEV³⁾, Sergei V. KASILOV^{1,4)},
 Winfried KERNBICHLER¹⁾, Henning MAASSBERG²⁾, Sadayoshi MURAKAMI⁵⁾,
 Victor V. NEMOV^{1,4)}, Donald A. SPONG⁶⁾, Victor TRIBALDOS⁷⁾

¹⁾*Institut für Theoretische Physik, Association EURATOM-ÖAW, TU-Graz, Austria*

²⁾*Max-Planck Institut für Plasmaphysik, Association EURATOM, Greifswald, Germany*

³⁾*Russian Research Center "Kurchatov Institute", Moscow, Russia*

⁴⁾*Institute of Plasma Physics, NSC-KhIPT, Kharkov, Ukraine*

⁵⁾*Department of Nuclear Engineering, Kyoto University, Kyoto, Japan*

⁶⁾*Oak Ridge National Laboratory, U.S. Department of Energy, USA*

⁷⁾*Laboratorio Nacional de Fusión, CIEMAT, Association EURATOM, Madrid, Spain*

October 11, 2007

The benchmarking of the mono-energetic particle transport coefficients for various stellarator configurations is completed, very good agreement was obtained by quite different codes (several Monte Carlo techniques, DKES, GSRACE and NEO). Such an extensive benchmarking for the bootstrap current coefficient is still lacking. The bootstrap current is an off-diagonal term in the neoclassical transport matrix and standard δf -Monte Carlo techniques are well suited only for the diagonal transport terms in stellarator configurations. This benchmarking is based on four different codes.

Keywords: ICNTS, neoclassical transport, stellarators, bootstrap current coefficient

1. Introduction

The *International Collaboration on Neoclassical Transport in Stellarators* (ICNTS) was initiated in 2000 for solving the linearised mono-energetic drift-kinetic equations

$$V^1(f_1) - C^p(f_1) = -\dot{r}$$

$$V^1(g_1) - C^p(g_1) = p v b.$$

Here, V^1 is the Vlasov term acting only in the flux surface (the radius, r , and the absolute velocity, v , are only parameters), C^p is the pitch-angle collision term (Lorentz form), $p = v_{\parallel}/v$, \dot{r} the radial component of the ∇B -drift velocity, and $b = B/B_0$ the normalised magnetic field strength. f_1 and g_1 are the *1st-order* distributions functions, i.e. the (small) deviation from the *0th-order* Maxwellian. The mono-energetic transport coefficients are defined by the following moments: $D_{11} = [\dot{r} f_1]$ is the particle diffusion coefficient, $D_{31} = v[p f_1]$ the bootstrap current coefficient, $D_{13} = [\dot{r} g_1]$ the Ware pinch coefficient, and $D_{33} = v[p g_1]$ the electric conductivity coefficient. Here, $[A] = \int \langle A \rangle dp$ where $\langle \dots \rangle$ denotes flux-surface averaging. Onsager symmetry leads to the relation $D_{31} = -D_{13}$. The 3×3 thermal transport matrix is obtained by energy convolution of the mono-energetic coefficients for different weights with respect to v .

The early ICNTS phase concentrated on the benchmarking of the D_{11} coefficient for the main stellarator configurations; see [1]. DKES (Drift-Kinetic Equation Solver) [2, 3] is based on a Fourier-Legendre expansion of both

author's e-mail: Henning.Maassberg@ipp.mpg.de

f_1 and g_1 in the 3D phase space and evaluates all mono-energetic diffusion coefficients depending on collisionality and radial electric field. MOCA [4] and DCOM [5] are full- f Monte Carlo codes evaluating D_{11} from the radial broadening of an ensemble of test particles in time following [6]. A δf MC technique [7] allows for a strictly local estimation of D_{11} , i.e. the radial drift velocity determines only the weight of the markers $w_f = \int \dot{r} dt$ for $r = const.$ This D_{11} benchmarking (also supported by other codes) is largely completed with very good agreement; the impact of the approximation of incompressible $E \times B$ flows for rather large radial electric fields, $E_r/vB > tr/R$, is analysed in [8].

Here, the scaling of the bootstrap current coefficient in the different collisionality regimes is briefly summarised: $D_{31} \propto 1/\nu^{*2}$ in the Pfirsch-schlüter regime, $D_{31} \propto 1/\nu^*$ in the plateau regime, and $D_{31} \rightarrow const.$ at very-low collisionalities, where $\nu^* = \nu R/vt$. This scaling holds both for stellarators and tokamaks.

2. The Numerical Tools

The bootstrap current coefficient evaluated by DKES could only be benchmarked with *standard* δf MC techniques either for an axisymmetric configuration or only for moderate collisionalities, so far. For estimating D_{11} and D_{33} , the marker equations $w_f = \int \dot{r} dt$ and $w_g = v \int p dt$ increase the weights of those markers which dominate the contribution to the corresponding coefficients at low collisionalities, i.e. ripple-trapped particles with large \dot{r} to D_{11} and passing particles with large p to D_{33} . The ripple-

trapped particle distribution function is nearly symmetric in p (allowing for a bounce-averaged treatment), but D_{31} is determined by the asymmetry in the passing particle distribution with rather small weights, w_f . Consequently, the large w_f of ripple-trapped particles leads to huge statistical problems for evaluating the D_{31} coefficient in stellarators at very-low collisionalities. This problem does not appear in axisymmetric configurations since \dot{r} is a periodic function along the banana orbit, and the tokamak D_{31} can be evaluated directly with δf -MC techniques; see e.g. [9]. The situation is equivalent for evaluating the Ware pinch coefficient: D_{13} is mainly determined by the trapped particles with small p whereas the far passing particles dominate in the marker weights w_g . This equivalence was found in direct δf -MC simulations of D_{31} and D_{13} : rather similar convergence problems appeared at the same (intermediate) collisionalities.

One possibility to overcome this *artificial noise* problem in δf -MC simulations of the bootstrap current coefficient is a filtering technique used in the VENUS- δf code [10, 11]. The strongly weighted ripple-trapped particles, i.e. the markers with large $|w_f|$, are omitted for evaluating D_{31} , and only barely trapped particles and passing particles contribute. This filtering technique based on δf bounds is equivalent to a forced localisation in r : if the radial drift of ripple-trapped particles exceeds a maximum radial displacement, their contribution to D_{31} is simply ignored. The main disadvantage of this approach, however, is the somewhat *artificial* definition of the δf bounds: the sensitivity of D_{31} on these bounds must be controlled for each magnetic configuration depending on the degree of drift-optimisation and fraction of ripple-trapped particles. At very-low collisionalities, VENUS- δf calculations are very time expensive.

Another approach used in the NEO-MC code, is based on the iterative evaluation of the distribution function in those phase space regions (e.g. close to the trapped-passing boundary) mainly contributing to the bootstrap current coefficient. The standard δf -MC methods are based on the *0th-order* Maxwellian, and δf must describe the full deviation without any iteration. Iterative re-discretisations of the distribution function in the relevant phase-space region for evaluating D_{31} by using this information for the next step reduce significantly the *artificial noise* introduced by the ripple-trapped particles [12]. The convergence of this method is equivalent to $\delta f \rightarrow 0$ within the iteration. Furthermore, a constant marker weight scheme with decreasing number of test particles is used for trapped particles leading to an additional statistical improvement for a fixed number of starting test particles. The variance (*noise*) in this method scales with the mean free path (instead of mean free path squared as in the standard method) and finally the computing time needed in NEO-MC for the same statistical error decreases by a factor proportional to the mean free path to the power $3/2$.

In addition, NEO-2 calculations of the bootstrap

current coefficient are included in the benchmarking. NEO-2 [13] integrates the linearised drift-kinetic equations along field lines for arbitrary collisionalities, however, the poloidal $E \times B$ drift cannot be included. In NEO-2, the Green's function technique in combination with an adaptive (*3rd-order*) conservative finite-difference discretisation scheme with respect to the normalised magnetic moment is applied which allows for high accuracy at low collisionalities (where DKES and both MC techniques become very time consuming due to the high localisation of the *1st-order* distribution functions in the 3D-phase space). Furthermore, NEO-2 is extended to the full linearised collision operator [14] (instead of the simplified Lorentz form of the pitch-angle collision term).

Finally, the collisionless asymptotic value of D_{31} is used for the benchmarking. In particular the axisymmetric value in the large aspect ratio limit, $\epsilon = r/R \rightarrow 0$, is used for normalisation. In this limit, the collisionless asymptote is easily obtained from the mono-energetic flux-friction relation for an axisymmetric configuration: for this case, the relation $\mathbf{B} \cdot \nabla B = -\tau \epsilon (\mathbf{B} \times \nabla B) \cdot \mathbf{e}_r$ holds, where \mathbf{e}_r is the radial unit vector, and all 3 mono-energetic transport coefficients are linked for small radial electric fields, E_r ; see [15]. The parallel electric conductivity is given by

$$D_{33}(\nu^* \rightarrow 0) = D_{33}(\nu^* \rightarrow \infty) - \frac{2\nu}{3\nu} f_t$$

where f_t is the trapped particle fraction

$$f_t = 1 - \frac{3}{4} \langle b_{\max}^2 \rangle \int_0^1 \frac{\lambda d\lambda}{\langle \sqrt{1 - \lambda b_{\max}} \rangle}$$

with $b_{\max} = B/B_{\max}$. In the large aspect ratio limit, $f_t \simeq 1.46\sqrt{\epsilon}$ for a tokamak with circular cross section, and

$$D_{31}(\nu^* \rightarrow 0) = \frac{2}{3} \frac{f_t}{\tau \epsilon} \simeq \frac{0.9733}{\tau \sqrt{\epsilon}}, \quad (1)$$

equivalent to the value given e.g. in [16] (here, the energy convolution with the Maxwellian leads to the factor $3/2$). This $D_{31}(\nu^* \rightarrow 0)$ is used for the normalisation of all bootstrap current coefficients in this benchmarking. DKES and NEO-2 calculations for an axisymmetric configuration have shown, that the convergence to this collisionless asymptote is rather slow, $\propto \sqrt{\nu^*}$, confirming the scaling of the size of the relevant boundary layer between trapped and passing particles; see e.g. [17]. Finally, D_{31} is independent of E_r in tokamaks as long as $E_r \ll \tau \epsilon B \nu$ holds.

In the stellarator *lmfp*-regime, D_{31} depends on E_r and ν^* in a rather complex manner. Nevertheless, for $\nu^* \rightarrow 0$, a purely geometrical factor, the Shaing-Callen limit [18, 19], is equivalent to the collisionless asymptote for axisymmetric configurations. However, the collisionalities in this benchmarking for stellarator configurations are in general too high to check the convergence of D_{31} to the collisionless Shaing-Callen limit. The convergence of

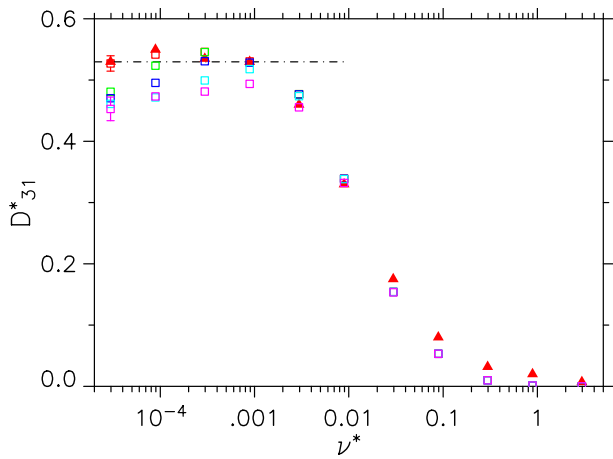


Fig. 1 Mono-energetic bootstrap current coefficients, D_{31}^* (normalised to the collisionless asymptote, eq.(1)), for NCSX vs. collisionality, ν^* . DKES (open squares) for $E_r/vB = 0$ (red), $1 \cdot 10^{-4}$ (green), $3 \cdot 10^{-4}$ (dark blue), $1 \cdot 10^{-3}$ (light blue), $3 \cdot 10^{-3}$ (magenta), and VENUS- δf (full triangles only for $E_r/vB = 0$). The Shaing-Callen value is given for reference (dot-dashed line).

D_{31} calculations at extremely low collisionalities (down to $\nu^* \sim 10^{-8}$ is accessible for the tokamak case) is very poor and requires huge computing times. Consequently, the Shaing-Callen limit is not seriously included in the D_{31} -benchmarking.

3. Benchmarking Results

Here, the benchmarking of the bootstrap current coefficient is discussed for 3 magnetic (vacuum) configurations at half the plasma radius: NCSX (*ncsx-2*), the “standard” LHD with $R = 3.75$ m (*lhd-375*), and the W7-X “standard” (*w7x-sc1*) configuration. NCSX is a quasi-axisymmetric configuration with high elongation [22], and the bootstrap current is expected to be rather similar to the equivalent tokamak. This LHD configuration represents a *classical* stellarator configuration [20]. Finally, the W7-X configuration is strongly drift-optimised, and the bootstrap current is minimised [21].

Fig. 1 shows the benchmarking results for DKES and VENUS- δf for NCSX. The impact of E_r is rather small, i.e. this quasi-axisymmetric configuration is similar to a tokamak with respect to the bootstrap current coefficient (but the radial transport coefficient, D_{11} , is dominated by ripple-trapped particles on which E_r has a large effect [1]). The fairly high NCSX elongation leads to the reduced D_{31}^* at the low collisionalities (for the normalisation in eq. (1), an axisymmetric configuration without elongation was assumed).

For the LHD configuration, all 4 codes contribute to the benchmarking shown in Fig. 2 (for a 1st benchmarking of VENUS- δf and DKES, see Ref. [23]). As in the NCSX case, the agreement of the quite different codes is very good. With E_r , the D_{31} at very low ν^* are decreased

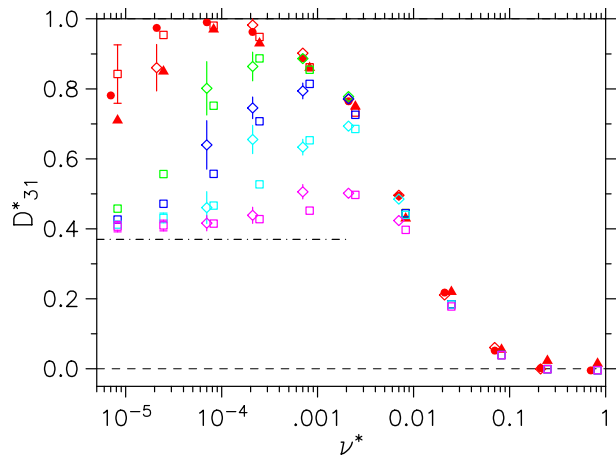


Fig. 2 Normalised mono-energetic bootstrap current coefficients, D_{31}^* , for LHD with $R = 3.75$ m vs. ν^* . DKES (open squares), VENUS- δf (full triangles), NEO-MC (open diamonds), and NEO-2 (full circles only for $E_r/vB = 0$) for $E_r/vB = 0$ (red), $3 \cdot 10^{-5}$ (green), $1 \cdot 10^{-4}$ (dark blue), $3 \cdot 10^{-4}$ (light blue), and $1 \cdot 10^{-3}$ (magenta); the Shaing-Callen value (dot-dashed line).

to the Shaing-Callen value. This reduction of the D_{31} with increasing E_r starts at the same ν^* as the reduction of the D_{11} coefficient (from the $1/\nu$ -regime). In the analytic theory [24], the coupling of the ripple-trapped particle distribution function and the passing particle distribution function changes in the transition from the $1/\nu$ - to the $\sqrt{\nu}$ -regime.

For this “standard” LHD configuration (without elongation), the D_{31} for $E_r = 0$ (except the very low ν^*) is rather similar to the equivalent tokamak (with circular cross section). An inward-shift of the magnetic axis leads to a drift-optimised stellarator configuration for $R = 3.60$ m [20] in the sense of σ -optimisation [25], and also the D_{31} for $E_r = 0$ at low ν^* are reduced by nearly a factor of 2, but the Shaing-Callen value is less affected. A stronger inward-shift (e.g. $R = 3.53$ m) further improves the *lmfp*-confinement (but violates the σ -optimisation), the bootstrap current coefficients are also reduced (found by DKES computations). Finally, an outward-shift of the magnetic axis results in negative D_{31} (reducing τ) in the plateau regime [23], the effect of the helical curvature terms in the B_{mn} -Fourier spectrum being increased.

The benchmarking for the W7-X “standard” configuration is shown in Fig. 3 with all 4 codes included. In this case, the D_{31}^* for only 3 E_r values are shown (more are available). Very time-expensive VENUS- δf computations at very low ν^* indicate the “convergence” of D_{31} to the Shaing-Callen value in the limit $\nu^* \rightarrow 0$ even for $E_r = 0$ (here, the statistical error of VENUS- δf is about 25%). At these low collisionalities, in particular DKES results have rather large errors (see Fig. 3), up to 2000 Fourier modes in the angle coordinates and 250 Legendre polynomials are used for the representation of the distri-

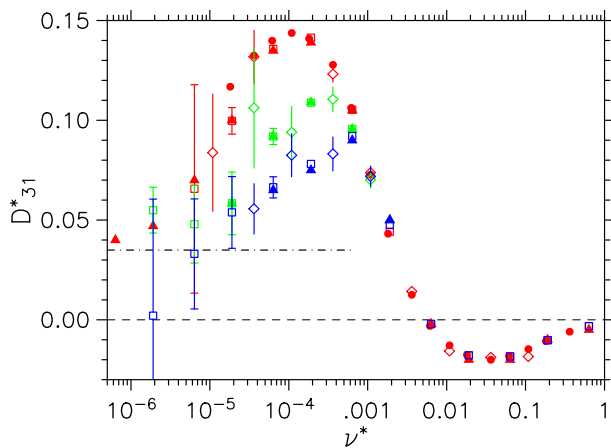


Fig. 3 Normalised mono-energetic bootstrap current coefficients D_{31}^* , for the W7-X “standard” configuration vs. ν^* . DKES (open squares), VENUS- δf (full triangles), NEO-MC (open diamonds), and NEO-2 (full circles) for $E_r/vB = 0$ (red), $1 \cdot 10^{-4}$ (green), and $1 \cdot 10^{-3}$ (dark blue); the Shaing-Callen value (dot-dashed line).

bution function), however, the D_{31}^* are fairly small (e.g. the relative errors are much smaller for the LHD configuration with large D_{31}^*). This W7-X example is similar to the LHD case where D_{31} is reduced with E_r (at larger E_r , however, D_{31} increases), however, the D_{31} are nearly one order of magnitude smaller than in the LHD case. These results confirm the W7-X optimisation criterium of minimised bootstrap current.

The variation of the toroidal mirror term in W7-X has a fairly strong impact on the bootstrap current coefficient; see [26]. The low-mirror configuration represents a *classical* highly-elongated stellarator configuration, and the D_{31}^* at low ν^* are increased by more than a factor of 2. On the other hand, the high-mirror configuration (with $B_{01}/B_{00} \simeq 0.1$) has the lowest D_{31}^* , but only at very small E_r . However, D_{31} increases with E_r to equivalent values as in the W7-X “standard” configuration, i.e. the high degree of bootstrap current minimisation in the high-mirror configuration is lost even for intermediate E_r .

4. Conclusions

For 3 quite different stellarator configurations, the benchmarking of the mono-energetic bootstrap current coefficient by 4 codes, i.e. DKES, VENUS- δf , NEO-MC and NEO-2, is performed and very good agreement was found. As a next step in the ICNTS activity, the impact of the violation of the momentum conservation in the simplified Lorentz form of the pitch-angle collision operator on the bootstrap current will be analysed in detail; see [27].

Acknowledgements

One of the authors, M. Isaev, thanks W.A.Cooper and T.M.Tran for the help and the support of the VENUS- δf

calculations. His work was supported by the CRPP-KIAM contract, by the MPG-grant, by Max-Planck Institut für Plasmaphysik, by NIFS/NINS under the Project of Formation of International Network of Scientific Collaboration (Japan), by the Fond National Suisse pour la Recherche Scientifique, and by the Departement of Atomic Science and Technology, RosAtom (Russia).

- [1] C.D. Beidler *et al.*, *30th EPS Conf. Plasma Phys. Contr. Fus., St Petersburg 2003*, http://epsppd.epfl.ch/StPetersburg/pdf/P3_002.pdf (2003).
- [2] S.P. Hirshman *et al.*, *Phys. Fluids* **29**, 2951 (1986).
- [3] W.I. van Rij and S.P. Hirshman, *Phys. Fluids* **B1**, 563 (1989).
- [4] V. Tribaldos, *Phys. Plasmas* **8**, 1229 (2001).
- [5] S. Murakami *et al.*, *Nucl. Fusion* **42**, L19 (2002).
- [6] A.H. Boozer and G. Kuo-Petravic, *Phys. Fluids* **24**, 851 (1981).
- [7] M. Schmidt, *29th EPS Conf. Plasma Phys. Contr. Fus., Montreux 2002*, http://epsppd.epfl.ch/Montreux/pdf/P4_112.pdf (2002).
- [8] C.D. Beidler *et al.*, *ICNTS - Impact of Incompressible $E \times B$ Flow in Estimating Mono-Energetic Transport Coefficients*, this workshop, (2007).
- [9] M. Sasinowski and A.H. Boozer, *Phys. Plasmas* **2**, 610 (1995).
- [10] O. Fischer *et al.*, *Nucl. Fusion* **42**, 817 (2002).
- [11] M.Yu. Isaev *et al.*, *Fusion Sci. Techn.* **50**, 440 (2006).
- [12] K. Allmaier *et al.*, *34th EPS Conf. Plasma Phys., Warsaw 2007*, P-4.041, (2007).
- [13] W. Kernbichler *et al.*, *32nd EPS Conf. Plasma Phys., Tarragona 2005*, http://epsppd.epfl.ch/Tarragona/pdf/P1_111.pdf (2005).
- [14] W. Kernbichler *et al.*, *33rd EPS Conf. Plasma Phys., Rome 2006*, http://epsppd.epfl.ch/Roma/pdf/P2_189.pdf (2006).
- [15] H. Maaßberg and C.D. Beidler, *31st EPS Conf. Plasma Phys. Contr. Fus., London 2004*, http://epsppd.epfl.ch/London/pdf/P1_100.pdf (2004).
- [16] A.H. Boozer and H.J. Gardner, *Phys. Fluids* **B2**, 2408 (1990).
- [17] F.L. Hinton and M.N. Rosenbluth, *Phys. Fluids* **16**, 836 (1973).
- [18] K.C. Shaing and J. Callen, *Phys. Fluids* **26**, 3315 (1983).
- [19] J.L. Johnson *et al.*, *Phys. Plasmas* **6**, 2513 (1999).
- [20] S. Murakami *et al.*, *Nucl. Fusion* **42**, L19 (2002).
- [21] H. Maaßberg *et al.*, *Phys. Fluids* **B5**, 3728 (1993).
- [22] G.H. Neilson *et al.*, *Phys. Plasmas* **7**, 1911 (2000).
- [23] M.Yu. Isaev *et al.*, *submitted to Plasma Fusion Res.* (2007).
- [24] C.D. Beidler and H. Maaßberg, *Plasma Phys. Control. Fusion* **43**, 1131 (2001).
- [25] H.E. Mynick *et al.*, *Phys. Rev. Lett.* **48**, 322 (1982).
- [26] N.B. Marushchenko *et al.*, *ECCD Scenarios for Different Configurations of the W7-X Stellarator*, this workshop, (2007).
- [27] C.D. Beidler *et al.*, *ICNTS - Benchmarking of Momentum Correction Techniques*, this workshop, (2007).